Journal of Imaging Science and Technology® 53(4): 040502–040502-8, 2009.

Computational Fluid Dynamics of Ionic Wind in a Corona Device in Electrophotography-(2)

Kazuhiro Mori and Hideki Okamoto
Key Technology Laboratory, Research and Technology Group, Fuji Xerox Co., Ltd., Nakai-machi, 259–0157 Ashigarakami-gun, Kanagawa, Japan
E-mail: kazuhiro.mori@fujixerox.co.jp

Masato Shiraishi
Evaluation Engineering Department, Fuji Xerox Engineering Co., Ltd., 243–0494, Ebina-shi, Kanagawa, Japan

Akihito Nishimura
Mechanical Development Department, Fuji Xerox Engineering Co., Ltd., 243–0494 Ebina-shi, Kanagawa, Japan

Abstract. *The ionic wind occurs with corona discharge. Knowledge of the ionic wind in a machine is necessary as a measure of the degradation of the image that originates from the generation products on corona discharge. The authors investigate the characteristics of the ionic wind in the neighborhood of a double-wire corona device through computational fluid dynamics to better understand this phenomenon. Various flow characteristics have been found. An inflow appears at the upper ventilation slit in the fan-off case. The primary flow diverges into some branches in a cross section. The authors can easily comprehend that this primary flow is derived from the schematic distribution of the body force. Several secondary vortices are induced by this flow at the same time. It is necessary to consider the effect of the grid electrode. Our numerical calculations correlate well with our experimental results by Particle Image Velocimetry. The primary flow appears also in a cross section on push-pull ventilation. Static pressure decreases along the wire. Large circulation occurs on the upstream side. Free powders that should contaminate the corona device move on the circulation. Large circulation thus has a close relation to contamination.*
[DOI: 10.2352/J.ImagingSci.Technol.2009.53.4.040502]

INTRODUCTION

Corona discharge is applied to the charging processes in electrophotography.[1] Corona devices create a corona current. The device consists of a corona producing wire (or wires) with grounded backing plate. Especially, corona devices are used in high-speed machines. However, corona devices cause ionic wind. The ionic wind occurs by the Coulomb force exerted on ions and from collisions of ions and neutral molecules of gas. Ions collide with the molecules of the air and transfer momentum to the air molecules. The ionic wind transports oxidation products, etc., which cause the degradation of the image as well as environmental problems.

The scorotoron is one type of corona device with a grid to control corona charging. The grid is set between a wire and a photoreceptor. In the previous paper,[2,3] we synthetically reported the basic characteristics of the ionic wind in a single-wire scorotron. A λ-shaped flow appears on a cross section in the fan-off case, and several vortices are induced by the λ-shaped flow. Static pressure decreases along the wire. We also found three-dimensional appearances. There is a countercurrent at both ends of the corona device in the fan-off case. Momentum is axially transported. Our numerical calculations correlated well with experimental results by Particle Image Velocimetry (PIV). The λ-shaped flow appears also in a cross section with a pull ventilation system, while the flow rate of the whole system is hardly changed. The ionic wind has an influence on the flow field in the neighborhood of the corona device. We could determine that the λ-shaped flow is derived from the schematic distribution of the body force, and we found that several vortices are induced by the λ-shaped flow.

Many investigations of corona discharge including the ionic wind have been conducted.[4–7] Yamamoto and co-workers[4] investigated three-dimensional electrohydrodynamics in the wire-duct electrostatic precipitator. In electrophotography, Nashimoto[5] reported the fundamental investigations of silicon oxide growth and the generation of reactive gases induced by corona discharge and proposed means to improve these phenomena. Zamankhan and co-workers[6,7] studied similar problems two dimensionally by coupled systems of electric and hydrodynamic governing equations.

Scharfe[8] stated that it is difficult to control and maintain free powders as early as 1984. Free powders cause contamination in machinery. Otsuka and Shiraishi[9] recently reported that dust carried onto a corona wire surface by airflow caused excessive discharge at that point, which thinned the wire. They prevented the recurrence of the failure by chang-

Received Aug. 8, 2008; accepted for publication Apr. 17, 2009; published online Jun. 2, 2009.
1062-3701/2009/53(4)/040502/8/$20.00.

ing the airflow system and the material of the wire. It is a reasonable conclusion that such contamination is related to degradation of the image. Small powders move on airflow. A designer expressed the opinion that the ionic wind "rampages" around a corona device. Thus polluted substances may unequally contaminate a corona device. Managing airflow and inflow of the polluted substances to corona devices is significant for preventing the degradation of the image. Therefore, knowledge of the flow field in the neighborhood of corona devices is necessary. However, it is impossible to accurately measure the flow field in a confined space. Physical phenomena occurring in confined spaces have generally been difficult to quantify. Moreover the influence of the electric field is strong in the neighborhood of a corona device. Measurement by a Pitot tube or a hot-wire anemometer is also difficult. PIV in machinery[10] has severe restrictions. One of these restrictions is an obstacle for capturing the image in a complicated structure. It is difficult to estimate the motion of tracer particles in internal flows. In addition, the ionic phenomenon essentially involves the coupling between the electric and fluid fields. Strictly speaking this coupling should be very weak; the electric field is hardly disturbed by the fluid field. Naturally, it might also be necessary to consider the temperature field in a practical case.[11] Therefore we have to study the complex phenomena in precision machinery based on the technology that uses electromagnetic and hydrodynamic force through computational fluid dynamics (CFD) to better understand these phenomena. In this paper, we take account of only the Coulomb force as the body force to calculate the momentum equation. We do not consider the buoyancy force and convective current.

Corona devices have infinite variety. Airflow systems around corona devices also have infinite variety. In this paper, we report behavior of the ionic wind in a double-wire scorotron. Below we discuss the analysis model and numerical conditions, and then describe the electric field and numerical calculations. The section on Electric Field and Fluid Calculations describes the electric field and numerical calculations. The body force due to the electric field is first calculated with the two-dimensional corona discharge simulation. Next, we use a computer program FLUENT ver.6.3.26 (FLUENT Inc., Lebanon, NH, USA) to calculate the steady three-dimensional flow field. We first treat phenomena in the fan-off case. The velocity profile produced by PIV at a ventilation slit and a primary flow are shown. Our numerical calculations correlate well with our experimental results. We then obtain velocity vectors, contours of static pressure in a middle plane, and marker particle path lines on push-pull ventilation system. The flow field exhibits a similar trend of behavior to the fan-off case. Finally, we summarize the basic characteristics of the ionic wind in the double-wire scorotron.

ANALYSIS MODEL IN OPEN SPACE AND CONDITIONS FOR NUMERICAL CALCULATIONS

Figure 1(a) shows an analysis model in open space. The axial direction of the wire is the z-direction. We assumed a

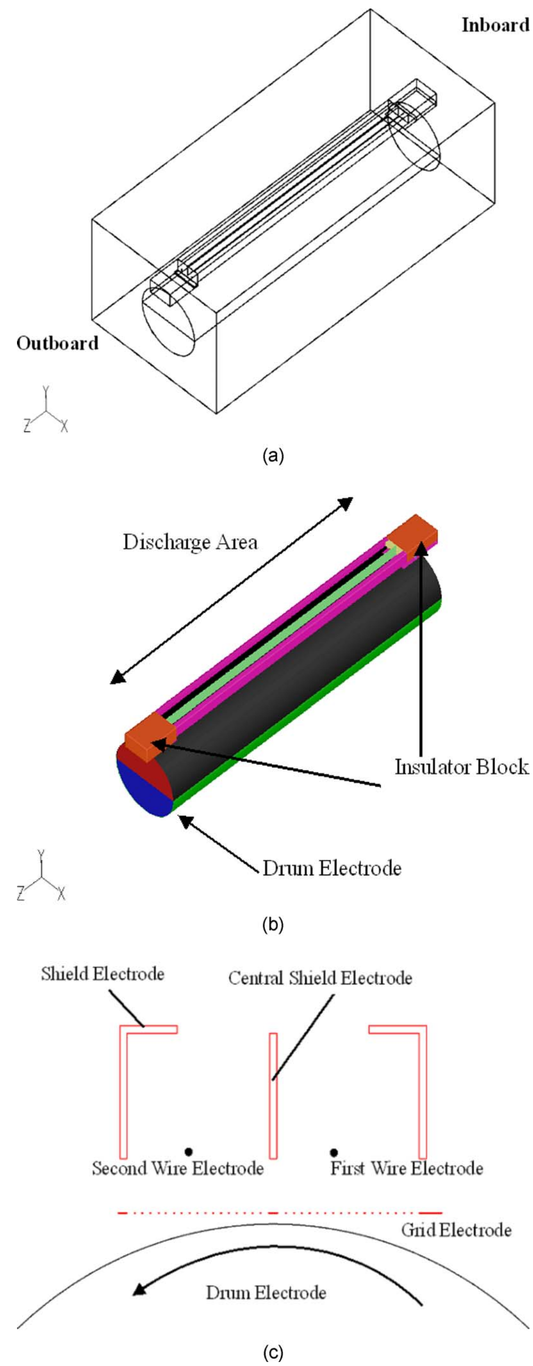

Figure 1. (a) Analysis model in the fan-off case. (b) Scorotron and photoreceptor. (c) Cross section diagram of the double-wire scorotron.

scorotron and a photoreceptor in open space. The outer surfaces are free slip walls. This model has about 1.81 million tetrahedral cells. The front of the model and the back of the model are called the outboard (front) side and the inboard (rear) side, respectively. The analysis model consists of a rectangular prism, 500 mm long, with cross-sectional dimensions of $200 \times 150\ \mathrm{mm}^2$.

Since we investigate the basic characteristics of the ionic wind in this paper, our studies have focused on the flow field in the neighborhood of the scorotron. Fig. 1(b) shows the scorotron and the photoreceptor. The scorotron is depicted as a rectangular solid attached to the cylindrical photorecep-

Table I. Geometrical parameters for the scorotron and the photoreceptor.

Width of corona device (m)	3×10^{-2}
Height of corona device (m)	2×10^{-2}
Length of corona device (m)	4×10^{-1}
Width of ventilation slit (m)	2×10^{-2}
Length of ventilation slit (m)	3×10^{-1}
Diameter of corona wire (m)	4×10^{-5}
Diameter of photoreceptor (m)	8×10^{-2}
Space between grid and photoreceptor (m)	1×10^{-3}

Table II. Electric parameters for the scorotron and the photoreceptor.

Wire voltage (V)	6000
Shield voltage (V)	800
Grid voltage (V)	800
Photoreceptor voltage (V)	0

tor. The photoreceptor rotates counterclockwise at 0.5 m/s. The scorotron has insulator blocks on both ends to stretch a wire electrode. There is a slit on the ceiling of the shield electrode for ventilation. In addition, a cross section in the neighborhood of the scorotron is shown in Fig. 1(c). The inner part of the scorotron is separated into two parts by a central shield electrode. Two wire electrodes are stretched in the inner side of the metal shield electrode. Both wire electrodes are offset 1.3 mm to the left side from the front view. The wire at the upstream side and the wire at the downstream side are called the first wire and the second wire, respectively. A grid electrode is set between the wire electrode and photoreceptor to help with uniform charging. The existence of the wire is negligible since the diameter of the wire is much smaller compared with the size of the flow field, and the mesh size is 0.15 mm in the neighborhood of the wire location. The grid is also neglected since a rate of openings is large. Table I shows geometrical parameters for the scorotron and the photoreceptor. Table II shows electrical parameters for the scorotron and the photoreceptor.

ELECTRIC FIELD AND FLUID CALCULATIONS

The ionic wind is a complex phenomenon.[11] The electric field, flow field, and temperature field mutually affect one another. Since the electrostatic force to the air is dominant, other effects are negligible in this analysis. Electrostatic force is calculated from the distribution of the electric field and charge density. These distributions are obtained by solving Gauss' law,

$$\frac{\partial(\varepsilon_{ij}E_j)}{\partial x_i} = \rho_e, \tag{1}$$

and the charge conservation equation,

$$\frac{\partial \rho_e}{\partial t} + \frac{\partial(\mu_e \rho_e E_j)}{\partial x_j} = 0, \tag{2}$$

where ε_{ij} is the permittivity, $E_i(i=1,2,3)$ represents the Cartesian components of the electric field E, ρ_e is the charge density, μ_e is the mobility of ion, and $x_i(i=1,2,3)$ represents the Cartesian coordinates. Here, we adopted the Einstein convention that whenever the index appeared twice in any term, we implied summation over the range of that index. Equations (1) and (2) are solved by the finite difference method. Charge and electric potential terms are coupled in Eqs. (1) and (2). Over time increments electric potential and charge distribution are alternately calculated until they reach a steady state. Then, we used the successive over-relaxation method to solve the matrix. The electric current produced by corona discharge is given by Sarma's assumption.[12] The charge density around the wire is set to keep the intensity of the electric field at threshold strength on its surface. The calculation of the electric field is represented on a cross section of the corona device since the geometry of the corona device is assumed to be uniform along the corona wire.

Distributions of the electric potential and the charge density are shown in Figures 2(a) and 2(b). Effect of charging on the photoreceptor is small inside the scorotron. The charges between the wire and the photoreceptor are dense. The charges outside the shield case are small. By use of the analysis model in Fig. 1(a), we show the behavior of the ionic wind in the fan-off case. Airflow is mainly induced by corona discharge.

We first calculated the body force with the two-dimensional corona discharge simulation. Next, FLUENT can numerically predict the flow field by considering the body force as the volumetric source term of the momentum equation.

FLUENT numerically solves the Navier-Stokes equations

$$\frac{\partial \rho}{\partial t} + \frac{\partial(\rho u_j)}{\partial x_j} = 0, \tag{3}$$

$$\frac{\partial(\rho u_i)}{\partial t} + \frac{\partial(\rho u_i u_j)}{\partial x_j} = -\frac{\partial p}{\partial x_i} + \frac{\partial}{\partial x_j}\left(\mu \frac{\partial u_i}{\partial x_j}\right) + F_i, \tag{4}$$

$$F_i = \rho_e E_i, \tag{5}$$

where ρ is the fluid density, p is the static pressure, $u_i(i=1,2,3)$ represents the Cartesian components of velocity u, $F_i(i=1,2,3)$ represents the Cartesian components of the body force derived from the ionic wind, and μ is the molecular viscosity of the fluid. We used constant values $\rho=1.204\ \mathrm{kg/m^3}$ and $\mu=1.808\times10^{-5}\ \mathrm{kg/m\ s}$. It is reasonable to assume the fluid is incompressible for this problem. Equation (5) is not necessarily accurate as static electric force is not fully converted to the driving force acting on neutral particles. The distribution of magnitude of the body force obtained by Eq. (5) is shown in Fig. 2(c); colors indicate the magnitude of the body force ($\mathrm{N/m^3}$). (Although the

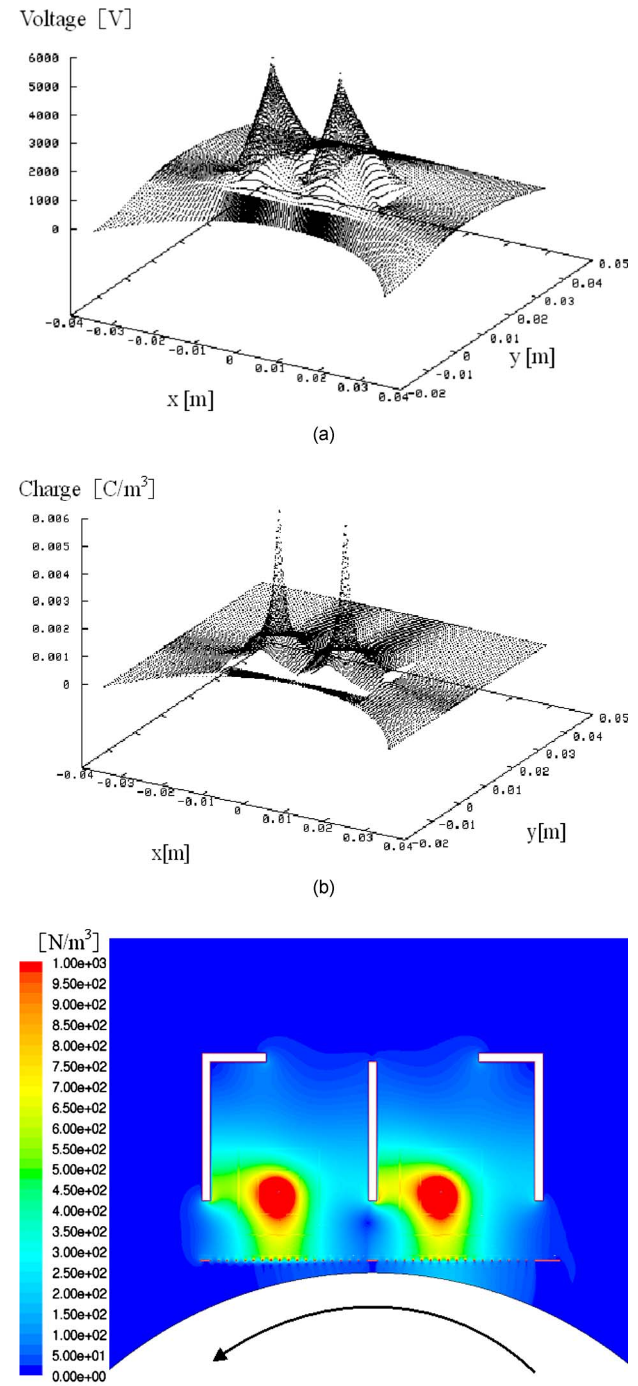

Figure 2. (a) Calculated distribution of the electric potential in the double-wire scorotron. (b) Calculated distribution of the charge density in the double-wire scorotron. (c) Calculated distribution of magnitude of the body force.

text makes reference to color, it will appear in color online only. The print figure will appear in black and white.)

The calculation grids around the wire electrode are very fine because the electric potential and charge distribution change drastically there. The grid spacing is set up with a minimum value of 10^{-6} m in the wire vicinity. Since the grids for airflow simulation are different from those used for the electric field simulation, the body force at the grid points are calculated by linear interpolation from the results of the electric field simulation. The body force is radial from the wire. The body force is strong between the wire and the photoreceptor. In contrast, the body force is weaker at the upper ventilation slit. By using the User Defined Function[13] to capture the body force as the volumetric source term, FLUENT calculates the three-dimensional flow field. We monitored a flow rate of the ventilation slit of the scorotron with the residuals for a convergence check.

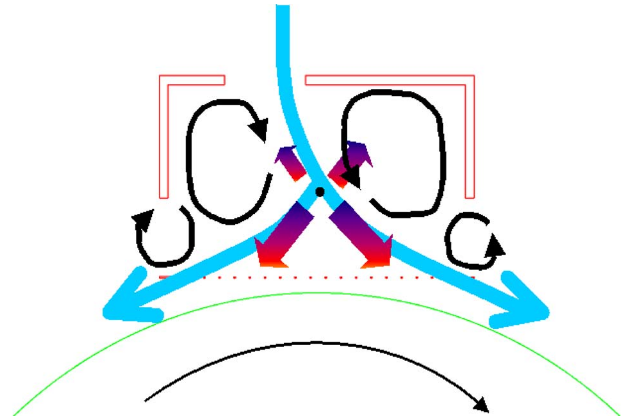

Figure 3. Schematic distribution of the flow field and the body force in the single-wire scorotron.

IONIC WIND PHENOMENON IN THE FAN-OFF CASE

We reported the ionic wind in a single-wire scorotron.[2,3] It was shown that the λ-shaped flow appeared in a cross section. Figure 3 shows the schematic distribution of the flow field and the body force in the single-wire scorotron. We could comprehend that the λ-shaped flow is derived from the schematic distribution of the body force. Also we found that several vortices are induced by the λ-shaped flow. In this paper, we extend the investigation to a double-wire scorotron.

PIV (Ref. 10) was applied to measure the ionic wind around a wire electrode. We consider a simple configuration, which consists of a corona device and a photoreceptor. The observation area is 60 mm from the edge of a photoreceptor drum in the longitudinal direction. The area is covered with outer walls, which are located more than 100 mm away from the wire electrode. The other experimental conditions are the same as the numerical analysis conditions. Smoke from an incense stick was used to provide tracer particles. Instantaneous λ-shaped flow is shown by tracer particles in a single-wire scorotoron in Figure 4(a). Fig. 4(b) also shows the primary flow by tracer particles in a double-wire scorotoron. Cavity regions appear downstream of the wire. Tracer particles cannot enter these cavity regions Figs. 4(a) and 4(b) implicitly show a significant possibility that certain free powders do not contaminate a wire on corona discharge. We show the calculated behavior of charged particles in Fig. 4(c). The particle diameter is 0.2 μm, and the particle charge is 3×10^{-13} C. Particles keep away from the wire. Cavity regions where particles cannot enter appear to

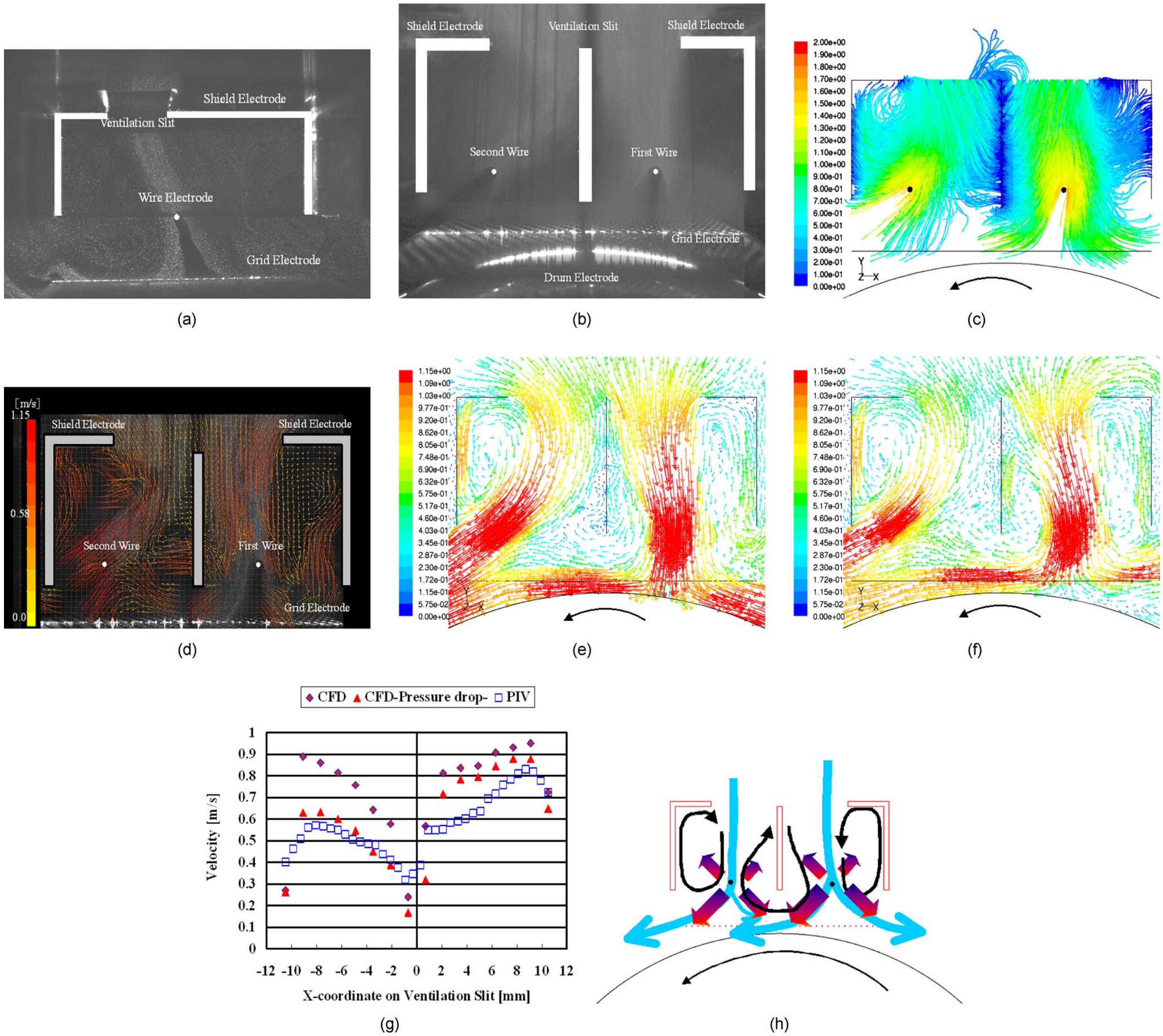

Figure 4. (a) Instantaneous λ-shaped flow shown by tracer particles in the single-wire scorotoron. (b) Primary flow shown by tracer particles in the double-wire scorotoron. (c) Calculated behavior of charged particles in the double-wire scorotoron. (d) Instantaneous velocity vectors by PIV in the double-wire scorotoron. (e) Calculated velocity vectors on corona discharge in the fan-off case in open space without considering effect of the grid electrode. (f) Calculated velocity vectors on corona discharge in the fan-off case in open space considering the effect of the grid electrode. (g) Velocity profile at the ventilation slit in the *x*-direction. (h) Flow field and schematic distribution of the body force in the double-wire scorotron.

be similar to the magnetosphere of the earth. Charge quantity is overestimated since we calculated particle orbit for a three-dimensional coarse mesh. We will accurately estimate the charge quantity by the two-dimensional fine mesh and discuss the motion of charged particles around a wire on corona discharge in near future.

Fig. 4(d) shows instantaneous velocity vectors by PIV. These vectors are colored by velocity magnitude (m/s). The captured images were analyzed by commercial software. We found that a complicated flow with vortices occurs.

Itoh and co-workers[14] examined laminar flow around a wire electrode induced by corona discharge in a system of wire and plate electrodes to obtain insight into the self-excited lateral oscillation of the wire electrode. Since the wire itself was negligible, the Reynolds number in large-scale space $R_E=5000$ was calculated. A reference velocity was defined by balancing the convection term and the Coulomb force, and a reference length was defined by setting the distance between the wire and the plate. They also investigated the fluid field around the wire by modeling the wire for the same phenomenon. The Reynolds number R_e is sufficiently small, and the flow field is laminar. We calculated the Reynolds number in large-scale space $R_E=2700$ for our model. We defined a reference velocity $U=2$ m/s and a reference length $L=0.02$ m. It is reasonable to assume that the flow field is laminar in the fan-off case.

Fig. 4(e) shows calculated velocity vectors in the neighborhood of the corona device. These vectors are colored by velocity magnitude (m/s). A flow rate through the ventilation slit is 6×10^{-3} kg/s.

By comparing Fig. 4(d) with Fig. 4(e), we immediately found different behavior of the flow field below the shield at the first wire side. So we have investigated effect of the grid. In this paper, we specifically consider the effect of pressure drop at the grid. Pressure drop, Δp, is defined by

$$\Delta p = -\left(\frac{\mu}{\alpha}v + \frac{1}{2}C_2\rho v^2\right)\Delta m, \qquad (6)$$

where μ is the fluid viscosity, $\alpha = 3.616 \times 10^{-10}$ m^2 is the permeability of the medium, $C_2 = 0$ 1/m is the pressure-jump coefficient, v is the velocity normal to the porous face, and $\Delta m = 1 \times 10^{-4}$ m is the thickness of the medium. We assumed the constant value for C_2 by estimating the pressure drop 1 Pa through the grid. Fig. 4(f) shows calculated velocity vectors in the neighborhood of the corona device including effect of the grid electrode.

Fig. 4(g) shows the velocity profile on the ventilation slit in the x-direction. The origin $x = 0$ is located in the center of the scorotron. The symbol ♦ indicates the CFD results, the symbol ▲ indicates the CFD results considering pressure drop through the grid, and the symbol □ indicates the PIV results. The CFD results considering pressure drop on the grid correlate better with the PIV results, especially for a balanced flow rate. For the two reasons mentioned above, it is necessary to consider the resistant effect of the grid in three-dimensional numerical simulation.

The λ-shaped flow is generated at the first wire side, the same as for a single-wire scorotron, and flow separations occur in the scorotoron. Our numerical calculations correlate well with our experimental results. Fig. 4(h) shows the flow field and the schematic distribution of the body force in the double-wire scorotoron. We could determine that this flow is also induced by the schematic distribution of the body force. Strong body force especially dominates for the primary flow. Also we found that several vortices are induced by this primary flow.

IONIC WIND PHENOMENON ON PUSH-PULL VENTILATION SYSTEM

In this section, we discuss the flow field with a push-pull ventilation system. A combination of push-pull ventilation is the most efficient form of ventilation for an electrophotographic engine. Yazaki[15] showed a push-pull ventilation system around a corona device in a copy machine. Figure 5(a) shows an analysis model for the case of push-pull ventilation. This model has about 5.5 million tetrahedral cells. The analysis model consists of a rectangular prism, 500 mm long, with cross-sectional dimensions of 230×140 mm^2.

Since we investigate the fundamental characteristics of the ionic wind in this paper, our studies have focused on the flow field in the neighborhood of the scorotron. Fig. 5(b) shows a cross section diagram in the neighborhood of the scorotron. Fresh air is provided from the right above the scorotron. An airflow system which leads ozone to the absorption filter on the inboard side to remove ozone is necessary. In addition, Fig. 5(c) shows a pull-ventilation system to collect vented substances. Marker, i.e., massless particle path lines, are colored by velocity magnitude (m/s). We consider a construction such as an airflow system with ducts, which drive air to the filtering element by a fan. A typical duct is 400 mm in length, 60 mm in width, and 70 mm in height. Velocity is prescribed as 3 m/s at the outlet boundary.

Fig. 5(d) also shows a push-ventilation system. This system has a risk of scattering airborne contaminants. Velocity is prescribed as 0.64 m/s at the inlet boundary. The other surfaces are no-slip walls. The duct has some baffles to direct the flow. Airflow is curved thereby and flows into the scorotoron from the right side, shown in Fig. 5(b). Finally air is exhausted to the inboard side by the pull ventilation system.

Flow rate of the ventilation slit for the scorotron was monitored with the residuals. We also considered the effect of the grid; the resulting pressure drop characteristics are described according to Eq. (6).

We show velocity vectors, contours of static pressure, and marker particle path lines. Fig. 5(e) shows velocity vectors in the neighborhood of the scorotron on corona discharge in the middle plane. These vectors are colored by velocity magnitude (m/s). Vortices were observed in the scorotron. We similarly calculated the Reynolds number in large-scale space $R_E = 2700$ for push-pull ventilation. We defined a reference velocity $U = 2$ m/s and a reference length $L = 0.02$ m. It is also reasonable to assume that the flow field is laminar with push-pull ventilation. Fig. 5(f) shows contours of static pressure (gauge pressure) in the middle plane on corona discharge. The contours are colored to indicate levels of static pressure (Pa). Static pressure rises at the region where the ionic wind collides with the photoreceptor. In contrast, static pressure decreases along the wire.

We will now discuss marker particle path lines in laminar flow. Fig. 5(g) shows marker particle path lines colored by velocity magnitude (m/s) of the flow field. Particles are injected from the surface of the ventilation slit. We found that large circulation occurs on the first wire side. Free powders move on the circulation and it has a close relation to contamination in the scorotron. Concentration of chemical species may be also dense.

Complex two-dimensional flow appears in most parts of the corona device, the same as for the fan-off case. The ionic wind locally has an influence on the flow field in the neighborhood of the double-wire scorotron with push-pull ventilation. The flow field in the neighborhood of the double-wire scorotron is, however, disturbed since the effect of the ventilation system is weak.

The characteristics in the wire direction are also important. This subject is under investigation in detail, and results will be reported in the near future.

SUMMARY

We have investigated the characteristics of the ionic wind in a double-wire scorotron. Especially, we have elucidated the

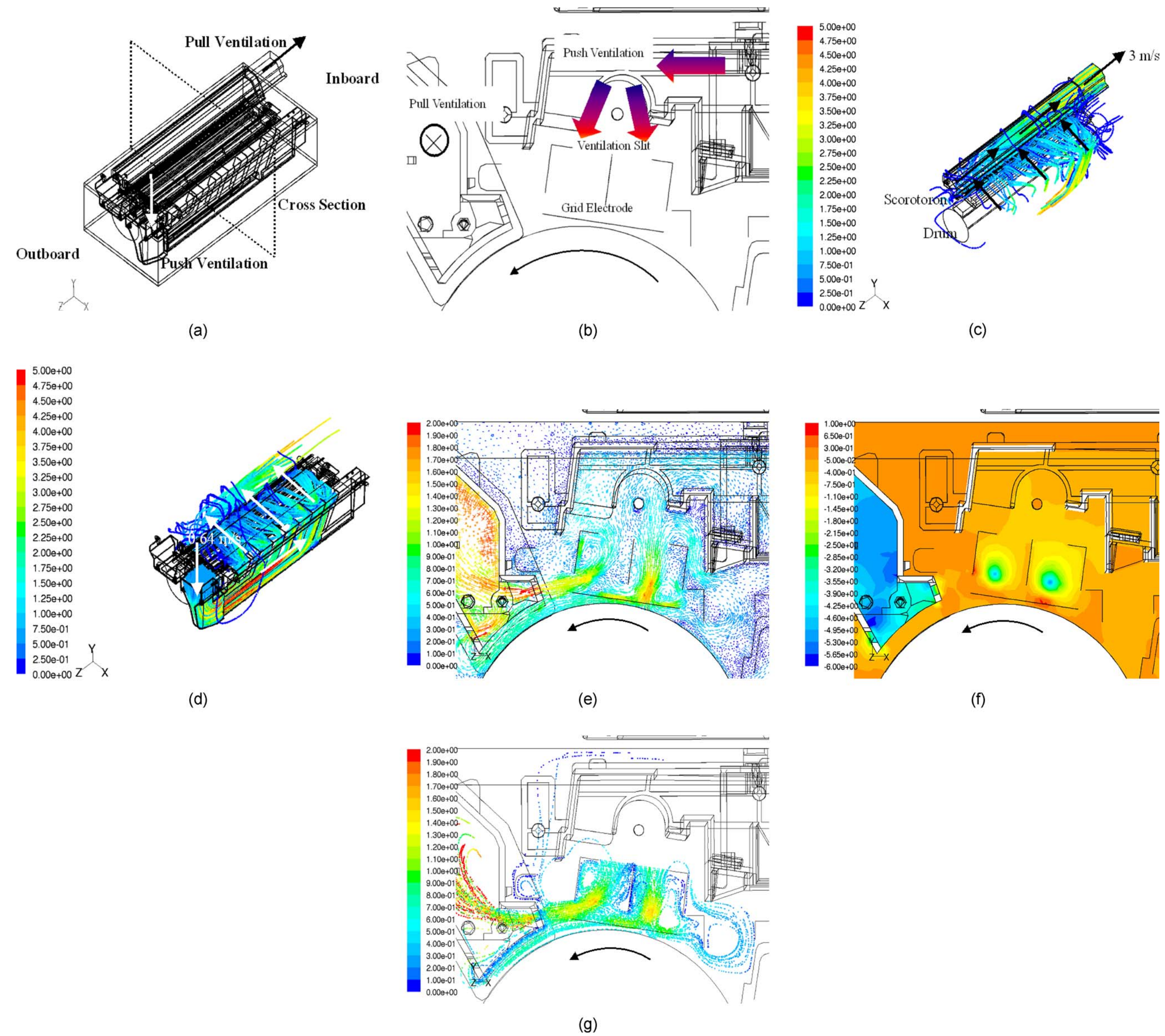

Figure 5. (a) Analysis model for push-pull ventilation. Cross section is shown in (b). (b) Cross section diagram in the neighborhood of the scorotron. Air flows into the scorotoron from the right side and is finally exhausted to the inboard side by pull ventilation system. (c) Pull ventilation system is separately shown. (d) Push ventilation system is separately shown. Some baffles in the duct direct the flow. (e) Calculated velocity vectors in the middle plane on corona discharge with push-pull ventilation. (f) Calculated contours of static pressure in the middle plane on corona discharge with push-pull ventilation. (g) Calculated marker particle path lines on corona discharge with push-pull ventilation. Marker particles are injected from the ventilation slit.

flow field in the neighborhood of the corona device. We have discovered the following:

- The primary two-dimensional flow appears in most parts of the scorotron. At the same time several secondary vortices are induced by this flow in the neighborhood of the double-wire scorotron. We can also comprehend that this flow is derived from the schematic distribution of the body force in the double-wire scorotron.
- Cavity regions that particles cannot enter appear on the downstream of the wire on corona discharge.
- Large circulation occurs on the upstream side. It has a close relation to contamination of the scorotron. Concentration of chemical species may be also dense.
- Our numerical calculations correlate well with our experimental results by PIV in the fan-off case.
- It is necessary to consider the effect of the grid electrode for three-dimensional numerical simulation.
- Static pressure rises at the region where the ionic wind collides with the photoreceptor. In contrast, static pressure decreases along the wire.
- The ionic wind has an influence on the flow field in the neighborhood of the double-wire scorotron with push-pull ventilation.

It is of importance to design machines considering control of the three-dimensional flow field. This fluid phenomenon is basically nonlinear and coupled. Corona devices can have infinite variety. Different phenomena occur with different system configuration. In two articles, for a single-wire and a double-wire scorotron we have shown the basic characteristics of the ionic wind and can confirm that our approach and findings are effective in designing corona devices.

REFERENCES

[1] E. M. Williams, *The Physics and Technology of Xerographic Processes* (Wiley, New York, 1984) p. 4.

[2] K. Mori, H. Okamoto, and N. Hirooka, "Computational fluid dynamics of ionic wind in a corona device in electrophotography-(1)", J. Imaging Sci. Technol. **48**, 465 (2004).

[3] K. Mori, "Computational fluid dynamics of precision machinery design", Doctoral thesis, Osaka City University, 2005, pp. 27–46.

[4] T. Yamamoto, M. Okuda, and M. Okubo, "Three-dimensional ionic wind and electrohydrodynamics of tuft/point corona electrostatic precipitator", IEEE Trans. Ind. Appl. **39**, 1602 (2003).

[5] K. Nashimoto, "Growth of silicon oxide and formation of reactive gases induced by corona discharge", Doctoral thesis, Nagoya Institute of Technology, 1989.

[6] P. Zamankhan, G. Ahmadi, and F. Fan, "Coupling effects of the flow and electric field in electrostatic precipitators", J. Appl. Phys. **96**, 7002 (2004).

[7] P. Zamankhan, G. Ahmadi, and F. Fan, "Variation of airflow and electric field in a corona device during charging of a moving dielectric substrate", J. Imaging Sci. Technol. **50**, 375 (2006).

[8] J. M. Scharfe, *Electrophotography Principles and Optimization* (Wiley and Sons, New York, 1984), p. 7.

[9] K. Otsuka and M. Shiraishi, "An analysis of corotron wire break", *Proc. of Reliability and Maintainability Symposium JUSE* (Union of Japanese Scientists and Engineers, Tokyo, Japan, 2005) p. 15 (in Japanese).

[10] N. Hirooka, Y. Ono, K. Mori, and N. Nakayama, "PIV measurements of airflow and ink mist motion around ink jet nozzles", *Proc. IS&T's NIP19: International Conference on Digital Printing Technologies* (IS&T, Springfield, VA, 2003) p. 284.

[11] A. Yabe, Y. Mori, and K. Hijikata, "EHD study of corona wind between wire and plate electrodes", AIAA J. **16**, 340 (1978).

[12] M. P. Sarma and W. Janischewskyj, "Dc corona on smooth conductors in air", Proc. IEEE **116**, 161 (1969).

[13] Fluent Inc., FLUENT 6.0 UDF Manual, 2001.

[14] Y. Itoh, M. Yoshizawa, T. Tsuzuki, and M. Sugawara, "Numerical analysis of the fluid field near the corona wire due to the corona discharge (the vortex formation and the fluid force on the wire)", Trans. Jap. Soc. Mech. Eng. (C) **64**, 4115 (1998) (in Japanese).

[15] N. Yazaki, "Air flow design of the color copiers for environmental", Ricoh Technical Report 25 (November 1999) (in Japanese); Available at http://www.ricoh.co.jp/about/business_overview/report/25/pdf/098103.pdf